Ultrafast Topological Engineering in Metamaterials

Renwen Yu [1,*] Rasoul Alaee [2] Robert W. Boyd,[2,3] and F. Javier García de Abajo [1,4,†]

[1]*ICFO-Institut de Ciencies Fotoniques, The Barcelona Institute of Science and Technology,
08860 Castelldefels (Barcelona), Spain*
[2]*Department of Physics, University of Ottawa, Ottawa, Ontario K1N 6N5, Canada*
[3]*The Institute of Optics, University of Rochester, Rochester, New York 14627, USA*
[4]*ICREA-Institució Catalana de Recerca i Estudis Avançats,
Passeig Lluís Companys 23, 08010 Barcelona, Spain*

Transient optical heating provides an efficient way to trigger phase transitions in naturally occurring media through ultrashort laser pulse irradiation. A similar approach could be used to induce topological transitions in the photonic response of suitably engineered artificial structures known as metamaterials. Here, we predict a topological transition in the isofrequency dispersion contours of a layered graphene metamaterial under optical pumping. We show that the contour topology transforms from elliptic to hyperbolic within a subpicosecond timescale by exploiting the extraordinary photothermal properties of graphene. This new phenomenon allows us to theoretically demonstrate applications in engineering the decay rate of proximal optical emitters, ultrafast beam steering, and dynamical far-field subwavelength imaging. Our study opens a disruptive approach toward ultrafast control of light emission, beam steering, and optical image processing.

Transient heating induced by laser pulse absorption has been intensely studied to induce phase transitions of interest such as metal-insulator transitions in VO_2 [1], amorphous-crystalline transitions in $Ge_2Sb_2Te_5$ [2], and charge-density-wave phase transitions in $1T$-TaS_2 [3], all of which hold strong potential for applications in next-generation electronic and optical data storage [4]. An interesting possibility arises when considering phase transitions in components of artificial structures known as metamaterials, which grant us access into a broader range of optical properties extending beyond those encountered in naturally occurring materials [5–9]. More recently, hyperbolic metamaterials have been found to exhibit an effective uniaxial anisotropic permittivity tensor that produces peculiar hyperbolic topology in the isofrequency dispersion contours and enables engineering of the decay rates of optical emitters [10,11], as well as hyperbolic waveguiding [12] and far-field subwavelength imaging [13,14], among other feats [15–17]. Hyperbolic metamaterials can be realized, for example, by stacking alternating layers of dielectric and plasmonic materials [10,11,18]. Among the latter, graphene offers unique properties, such as remarkably low optical losses [19,20] and the ability to tune its optical conductivity through electrical gating [21–24]. In fact, hyperbolic metamaterials based on layered graphene-dielectric stacks [25–28] are being intensely explored as a platform for the aforementioned applications [27] involving infrared light, exploiting a topological transition of the isofrequency contour

induced by tuning the doping level of graphene through electrical gating.

When subject to ultrafast optical pulse irradiation, the energy absorbed by graphene is first deposited in its conduction electrons, which can reach an elevated temperature (> 1000 K [29,30]) that remains high during ~ 0.5–1 ps before transferring a substantial fraction of heat to the lattice [31–33]. This is due to the small electronic heat capacity [34,35] and the weak electron-phonon coupling [35,36] of graphene. A strong thermo-optical response is then triggered through the temperature dependence of the graphene optical conductivity. Consequently, we expect that topological transitions of isofrequency contours could be triggered in metamaterials formed by layered graphene-dielectric stacks under ultrafast optical pumping, similar to light-driven phase transitions in natural materials. Importantly, the concept of photothermally induced topological transition can be readily applied to other metamaterials containing any material with optical properties that depend strongly on temperature [2,37–39]. In graphene-based metamaterials, the topological transition can be ultrafast because of the exceptionally small electronic heat capacity of graphene [35,40], which outperforms other materials [2,38] or mechanisms (e.g., electrical doping [25–27]) in terms of the transition speed. We further note that it is experimentally challenging to dope multiple graphene layers by electrical gating.

In this Letter, we theoretically investigate ultrafast photothermal manipulation of a topological transition in layered
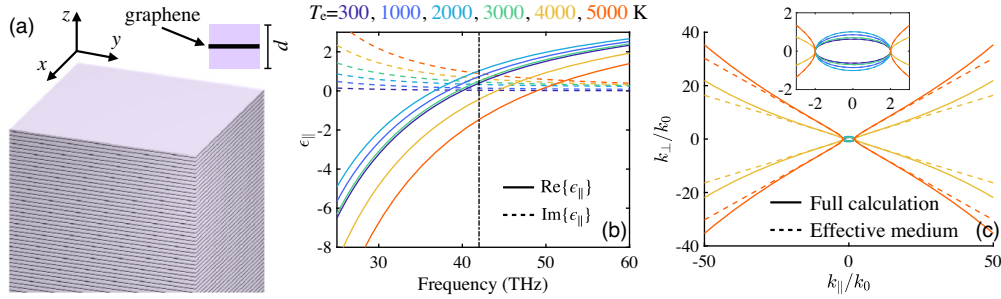
FIG. 1. (a) Schematic of a metamaterial made of graphene-dielectric stacks. The right inset shows a vertical unit cell with graphene located in the center. In this work, we take a unit cell thickness $d = 20$ nm, a permittivity of the dielectric $\epsilon_d = 4$, and a graphene Fermi energy $E_F = 0.4$ eV. (b) Real and imaginary parts of the effective in-plane (i.e., for polarization in the $x - y$ plane) permittivity $\epsilon_\parallel$ as a function of optical frequency at different graphene electron temperatures T_e, as indicated by labels. (c) Isofrequency dispersion contours at a fixed frequency of 42 THz [indicated as a dash-dotted vertical line in panel (b)] for different electron temperatures. We compare results obtained from electromagnetic numerical simulations (solid curves) and an effective medium model (dashed curves). The topology of the contour transforms from elliptic to hyperbolic as T_e increases.

metamaterials composed of graphene-dielectric stacks driven by light absorption in graphene. Based on a realistic description of the temperature-dependent optical properties of graphene, in combination with the spatiotemporal heat flow within its electron and lattice subsystems under ultrafast laser pumping, we predict a topological transition of the isofrequency dispersion contours of the metamaterial in the infrared domain, whereby the topology transforms from elliptic to hyperbolic within an ultrafast timescale. We show that the spatiotemporal dynamics of this topological transition can be probed by a delayed free electron beam and further find the transient hyperbolic phase to last ∼1 ps. Our results enable several exotic phenomena in the ultrafast regime, such as dynamical engineering of the decay rate of optical emitters in the vicinity of the metamaterial, as well as directional beam steering by carving the metamaterial into a cylindrical lens, which we show to be useful for subwavelength far-field image encoding or decoding.

In Fig. 1(a), we sketch a metamaterial composed of graphene-dielectric stacks with graphene located in the center of the dielectric-graphene-dielectric unit cell (see inset). We take a unit cell thickness $d = 20$ nm, a permittivity of the dielectric material $\epsilon_d = 4$, and a graphene Fermi energy $E_F = 0.4$ eV throughout this work. Given the small value of d compared to the infrared light wavelengths considered in this work, an effective permittivity should accurately describe the dielectric response of the metamaterial. Because of the system symmetry, we then have an effective uniaxial anisotropic material with two different permittivities $\epsilon_\parallel$ and $\epsilon_\perp$ along in-plane (x-y plane) and out-of-plane (z axis) directions, respectively. Additionally, due to the two-dimensional nature of graphene, we have $\epsilon_\perp = \epsilon_d$. Note that optical-pulse pumping can elevate the temperature of graphene electrons up to ∼5000 K within an ultrafast timescale [31,32,41]. We present the spectral dependence of the in-plane effective permittivity $\epsilon_\parallel = \epsilon_d + i4\pi\sigma/\omega d$ for different electron temperatures T_e in Fig. 1(b),

where σ is the temperature-dependent surface conductivity of graphene and ω is the angular frequency. It should be noted that the epsilon-near-zero frequency (Re$\{\epsilon_\parallel\} = 0$, see solid curves) is first redshifted and then blueshifted as T_e is increased, which is a consequence of the nontrivial T_e dependence of the graphene chemical potential [36]. More specifically, the Re$\{\epsilon_\parallel\} = 0$ condition leads to a frequency $\approx \sqrt{4e^2\mu^D/\hbar^2\epsilon_d d}$, where μ^D is the temperature-dependent effective Drude weight in the graphene conductivity (see Supplemental Material (SM) [42] for more details). Additionally, Im$\{\epsilon_\parallel\}$ (dashed curves) increases with T_e as a consequence of the enhancement in the inelastic scattering rate of graphene electrons [50].

We now explore the isofrequency dispersion contours at different electron temperatures for p-polarized electromagnetic fields, which are shown in Fig. 1(c) at a frequency of 42 THz [indicated by a vertical black dash-dotted line in Fig. 1(b)]. The figure reveals two distinct regimes represented by the topology of the isofrequency contour, which evolves from elliptic to hyperbolic as T_e increases. Specifically, within the $T_e = 300$–3000 K range, the isofrequency contour remains elliptic, despite some variations in shape. When T_e is further increased, a dramatic variation of the contour topology occurs, which results in an emerging hyperbolic metamaterial because Re$\{\epsilon_\parallel\} < 0$ when $T_e > 3000$ K. These results demonstrate that controlling T_e in graphene can be an efficient and ultrafast route toward inducing topological transitions through optical pulse pumping. Incidentally, we compare the isofrequency dispersion contours calculated with the transfer matrix method in Fig. 1(c) (solid curves) with those obtained from the effective medium theory (dashed curves), as determined by

$$\frac{k_\parallel^2}{\epsilon_\perp} + \frac{k_\perp^2}{\epsilon_\parallel} = k_0^2, \tag{1}$$

where k_0 is the free-space light wave vector, while $k_\parallel$ and $k_\perp$ are the wave vectors along in- and out-of plane directions, respectively. We attribute the discrepancies between these two methods observed at large values of $k_\parallel$ to the invalidity of the effective medium model when $k_\parallel d \ll 1$ no longer holds.

A promising application of hyperbolic metamaterials relates to their ability to manipulate the decay rate of proximal emitters by enhancing the local density of optical states (LDOS) [11], which is given by [51,52]

$$\frac{\text{LDOS}_\parallel}{\text{LDOS}_0} = 1 + \frac{3}{4}\int_0^\infty \frac{k_x dk_x}{k_0^3}\text{Re}\left\{\left(\frac{k_0^2 r_s}{k_z} - k_z r_p\right)e^{2ik_z z_0}\right\}$$

(2)

and

$$\frac{\text{LDOS}_\perp}{\text{LDOS}_0} = 1 + \frac{3}{2}\int_0^\infty \frac{k_x^3 dk_x}{k_0^3}\text{Re}\left\{\frac{r_p}{k_z}e^{2ik_z z_0}\right\}$$

(3)

for in- and out-of-plane polarization, respectively, where $k_z = \sqrt{k_0^2 - k_x^2}$, z_0 is the separation distance between the emitter and the metamaterial surface, and r_s and r_p are the reflection coefficients at the metamaterial-air interface for s and p polarizations. These expressions are normalized to the projected LDOS in free space $\text{LDOS}_0 = \omega^2/3\pi^2 c^3$, where c is the speed of light. The temperature dependence of the LDOS enhancement is presented in Fig. 2 at a distance $z_0 = 50$ nm above the upper surface of the metamaterial [see inset in Fig. 2(a)]. A large LDOS enhancement ($> 10^3$) is found as a result of strong confinement of the photonic modes supported by the metamaterial. In general, as the electron temperature T_e increases, the spectral range with high LDOS extends to lower frequencies. More specifically, an enhancement of 2 orders of magnitude can be obtained at ~ 48 THz when increasing T_e (see color-coded labels) due to the topological transformation of the isofrequency contour described in Fig. 1. This means that one can control the emitter decay rate in an ultrafast manner through raising the electron temperature by means of optical pulse pumping. Our findings are robust against the number N of vertical unit cells composing the metamaterial film for a dipolar emitter polarized parallel [Figs. 2(a),(b)] or perpendicular [Figs. 2(c), (d)] to the surface. The deviation between the results calculated by using the transfer matrix method (solid curves) or the effective medium model (dashed curves) are again related to the mismatch at large values of $k_\parallel$. The sharp change in the LDOS spectra indicates the occurrence of the topological transition at different light frequencies for different T_e. Note that this change becomes smoother at higher electron temperatures mainly due to an increase in the inelastic scattering rate τ^{-1} of graphene electrons [50]. More details about the calculation of r_s and r_p, the τ dependence of the LDOS, and the relative variation of the
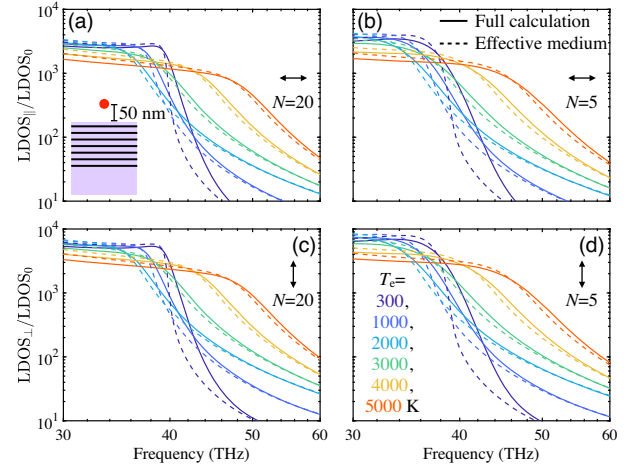
FIG. 2. (a),(b) Temperature-dependent enhancement of the LDOS as a function of frequency for metamaterials composed of different numbers N of vertical periods. The probing point dipole has in-plane polarization and is placed 50 nm away from the surface. (c),(d) Same as (a),(b) for out-of-plane polarization. We compare the results obtained from a fully numerical calculation (solid curves) with the effective medium model (dashed curves).

LDOS when increasing T_e can be found in the SM [42]. Naturally, controlling the lifetime of proximal emitters through a topological transition can be also achieved by exploring different light frequencies [10].

In order to resolve the ultrafast spatial and temporal dynamics of the topological transition, an electron probe moving in free space can be employed to spatially image the topological transition in the so-called aloof configuration [53] after a short optical pulse pumping, as illustrated in Fig. 3(a). This type of experiment can be performed with state-of-the-art ultrafast electron microscopes, relying on pulsed optical pumping and electron probing [54–58]. The probe electron can provide direct information about the topological transition through the EELS signal, the probability of which is given by [53]

$$\frac{\Gamma(\omega)}{L} = \frac{2e^2}{\pi\hbar v^2}\int_0^\infty \frac{dk_y}{k_\parallel^2}\text{Re}\left\{\left(\frac{k_y^2 v^2}{k_z^2 c^2}r_s - r_p\right)k_z e^{2ik_z z_0}\right\}, \quad (4)$$

where L is the length of the electron trajectory, v is the electron velocity, z_0 is the separation distance between the electron beam and the metamaterial surface, $k_\parallel = \sqrt{\omega^2/v^2 + k_y^2}$, and $k_z = \sqrt{k_0^2 - k_\parallel^2}$. We note that the loss probability given by Eq. (4) bears a close relation to the momentum decomposition of LDOS along the electron trajectory [59]. Here, we set the electron velocity to $v = 0.5c$ (~ 100 keV energy) and the separation to $z_0 = 50$ nm. We further consider a Gaussian pump pulse of 100 fs duration, 2 mJ/cm^2 fluence, and 600 nm beam width in the visible range. Following optical pumping of a metamaterial film composed of $N = 10$ vertical unit cells,
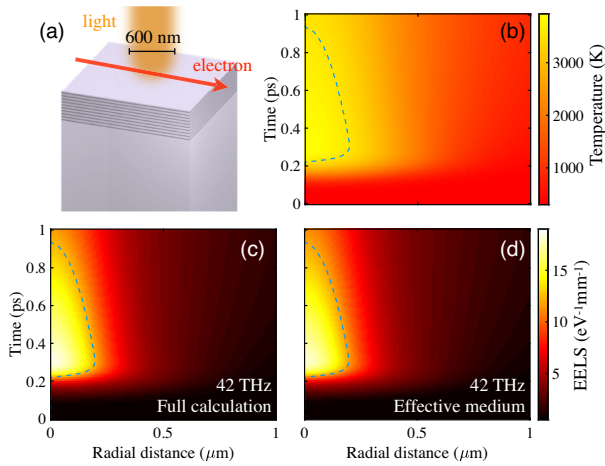
FIG. 3. (a) Schematic of a pump-probe configuration involving a normally incident optical pump pulse and a probing free electron beam passing parallel to the surface at a distance of 50 nm. We consider a metamaterial film consisting of $N = 10$ vertical periods. (b) Calculated spatiotemporal dynamics of the graphene electron temperature assumed to be uniform across the thickness of the thin metamaterial film. The spatial coordinate indicates the distance to the center of the axisymmetric optical Gaussian pulse (600 nm beam width). (c),(d) Spatiotemporal dynamics of the EELS signal for an electron frequency loss of 42 THz, as obtained through full electromagnetic calculations (c) or using an effective medium model for the metamaterial (d). The occurrence of the topological transition of the isofrequency contour, taking place at $T_e \approx 3560$ K for the optical frequency under consideration, is indicated by blue-dashed curves in (b)–(d), which enclose the spatiotemporal domain characterized by a hyperbolic response.

we calculate the resulting spatiotemporal dynamics of the electron temperature using a two-temperature model (see SM [42] for details). The results are shown in Fig. 3(b), where the in-plane radial distance is referred from the Gaussian beam center. The electron temperature reaches a maximum value ∼4000 K at the beam center immediately after pumping and then decreases as time evolves. In a way that is consistent with its intimate relation to the LDOS, the spatiotemporal dynamics of the EELS signal follows closely that of T_e at a fixed frequency loss of 42 THz, as shown in Figs. 3(c), (d), where the results obtained from the effective medium model [Fig. 3(d)] match quite well those obtained from the full calculation [Fig. 3(c)]. The blue-dashed curves in Figs. 3(b)–(d) enclose a spatiotemporal regime in which the isofrequency contour is transformed to be hyperbolic, giving rise to an enhanced EELS signal. Within ∼1 ps timescale, the topology of the isofrequency contour transforms from elliptic to hyperbolic and then back to elliptic, thus encompassing an ultrafast topological transition.

As a final example of application of the ultrafast topological transition discussed above, we investigate light steering and superresolution imaging. It has been demonstrated that hyperbolic metamaterials with nearly flat
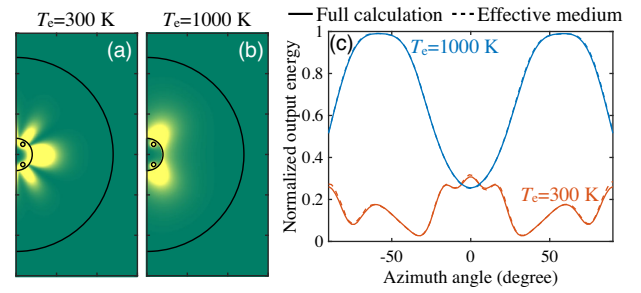
FIG. 4. (a) Spatial distribution of the optical energy density in a plane perpendicular to a cylindrical metamaterial lens (bounded by the two black semicircles of radii $R_1 = \lambda/5$ and $R_2 = 6\lambda/5$, respectively) at room temperature $T_e = 300$ K when it is excited by two magnetic current sources (represented by two small black circles close to the inner lens surface) separated by a subwavelength distance $l = \lambda/4$. We consider a light wavelength $\lambda = 7.8$ μm (i.e., 38.2 THz frequency). The permittivity of the medium inside the inner circle and outside the outer one is taken to be 1 and 4, respectively. (b) Same as (a) when the graphene electron temperature in the metamaterial is raised to $T_e = 1000$ K. (c) Normalized far-field emitted energy as a function of azimuthal angle, spanning a range from −90° to 90°, at the two electron temperatures considered in (a),(b). We compare results obtained from full electromagnetic simulations (solid curves) and the effective medium model (dashed curves).

isofrequency dispersion contours are capable of producing subwavelength imaging of a point source [13,14]. Here, we study the radiated energy distribution emanating from two magnetic line current sources [black full circles in Figs. 4(a),(b), separated by $\lambda/4$, where $\lambda = 7.8$ μm is the optical frequency corresponding to a 38.2 THz frequency]. These sources are placed in front of a cylindrical lens made of a curved version of the layered graphene-dielectric under consideration. At room temperature $T_e = 300$ K, the isofrequency contour is indeed hyperbolic at 38.2 THz [see Fig. 1(b)]. However, because of the curved nature of the isofrequency contour, several guided modes are excited with different wave vectors k_r along the radial direction [60]. As a result, multiple lobes show up in the spatial distribution of the energy densities [Fig. 4(a)], which also transmit into the far field [red curves in Fig. 4(c)]. When T_e is increased to 1000 K, the so-called canalization condition [61,62] Re$\{\epsilon_\theta\} \approx 0$ is satisfied, leading to a nearly flat isofrequency contour. Here, ϵ_θ is the effective permittivity of the cylindrical lens along the azimuthal direction. This results in two highly directive lobes in the spatial distribution of the energy density [Fig. 4(b)], thus demonstrating that the cylindrical lens is capable of ultrafast beam steering driven by the transient elevation of T_e rising upon optical pulse pumping. Additionally, two clear angular peaks associated with those two individual point sources can be identified in the far-field regime [see blue curves in Fig. 4(c)], further supporting the potential for far-field subwavelength imaging in a dynamical and ultrafast manner. Once more, the azimuthal distribution of the far

field signal obtained from full numerical simulations (solid curves) matches well the result obtained from the effective medium model (dashed curves), as shown in Fig. 4(c). In principle, the steering angle can be determined by the position of the point sources as well as the geometric parameters of the metamaterial lens. In the design shown in Fig. 4, the steering angle can be changed from 0° to ∼60° when the topological transition occurs (see more details in SM [42]). Our results further suggest a novel subwavelength image encoding-decoding mechanism, whereby an elevated electron temperature induced by optical pumping is the key to resolve encoded subwavelength images in the far-field regime.

In summary, we have shown that transient heating can significantly modify the topology of the isofrequency dispersion contours in metamaterials formed by layered graphene-dielectric stacks by exploiting the remarkably small electronic heat capacity of graphene, which allows us to efficiently elevate the electron temperature through ultrafast optical pumping. By examining the spatiotemporal dynamics of the EELS signal obtained by using an electron-beam probe, we have found that the contour topology can transform between elliptic and hyperbolic shapes within a subpicosecond timescale, that is, the characteristic time over which the elevated electron temperature evolves in real space. We can thus manipulate the LDOS enhancement in the proximity of the metamaterial, reaching variations in the calculated LDOS of a few orders of magnitude at the frequency in which this topological transition appears. Additionally, this type of transition enables ultrafast beam steering, which we have illustrated by illuminating a cylindrical lens made of metamaterials with two line sources, in which dynamical far-field subwavelength imaging has been demonstrated. Compared to previous studies on ultrafast beam steering [63,64] and spontaneous emission control [65–67], photo-thermal manipulation of the isofrequency contour topology provides a new avenue to enter the subpicosecond regime. Furthermore, both beam steering and spontaneous emission can be actively controlled by using the same nanostructure. Our findings open a promising route toward ultrafast control of light emission, beam steering, and optical image processing.

*Corresponding author.
renwen.yu@icloud.com
†Corresponding author.
javier.garciadeabajo@nanophotonics.es

[1] R. Xie, C. T. Bui, B. Varghese, Q. Zhang, C. H. Sow, B. Li, and J. T. Thong, Adv. Funct. Mater. 21, 1602 (2011).

[2] I. Friedrich, V. Weidenhof, W. Njoroge, P. Franz, and M. Wuttig, J. Appl. Phys. 87, 4130 (2000).

[3] K. Haupt, M. Eichberger, N. Erasmus, A. Rohwer, J. Demsar, K. Rossnagel, and H. Schwoerer, Phys. Rev. Lett. 116, 016402 (2016).

[4] M. Wuttig and N. Yamada, Nat. Mater. 6, 824 (2007).

[5] V. G. Veselago, Sov. Phys. Usp. 10, 509 (1968).

[6] J. B. Pendry, Phys. Rev. Lett. 85, 3966 (2000).

[7] N. Fang, H. Lee, C. Sun, and X. Zhang, Science 308, 534 (2005).

[8] D. Schurig, J. J. Mock, B. J. Justice, S. A. Cummer, J. B. Pendry, A. F. Starr, and D. R. Smith, Science 314, 977 (2006).

[9] A. A. Lalayalan, K. S. Bagdasaryan, P. G. Petrosyan, K. V. Nerkararyan, and J. B. Ketterson, J. Appl. Phys. 91, 2965 (2002).

[10] H. N. Krishnamoorthy, Z. Jacob, E. Narimanov, I. Kretzschmar, and V. M. Menon, Science 336, 205 (2012).

[11] D. Lu, J. J. Kan, E. E. Fullerton, and Z. Liu, Nat. Nanotechnol. 9, 48 (2014).

[12] V. A. Podolskiy and E. E. Narimanov, Phys. Rev. B 71, 201101(R) (2005).

[13] Z. Jacob, L. V. Alekseyev, and E. Narimanov, Opt. Express 14, 8247 (2006).

[14] Z. W. Liu, H. Lee, Y. Xiong, C. Sun, and X. Zhang, Science 315, 1686 (2007).

[15] L. Ferrari, C. Wu, D. Lepage, X. Zhang, and Z. Liu, Prog. Quantum Electron. 40, 1 (2015).

[16] P. Huo, S. Zhang, Y. Liang, Y. Lu, and T. Xu, Adv. Opt. Mater. 7, 1801616 (2019).

[17] Z. Guo, H. Jiang, and H. Chen, J. Appl. Phys. 127, 071101 (2020).

[18] A. Poddubny, I. Iorsh, P. Belov, and Y. Kivshar, Nat. Photonics 7, 948 (2013).

[19] A. Woessner, M. B. Lundeberg, Y. Gao, A. Principi, P. Alonso-González, M. Carrega, K. Watanabe, T. Taniguchi, G. Vignale, M. Polini et al., Nat. Mater. 14, 421 (2015).

[20] G. X. Ni, A. S. McLeod, Z. Sun, L. Wang, L. Xiong, K. W. Post, S. S. Sunku, B.-Y. Jiang, J. Hone, C. R. Dean et al., Nature (London) 557, 530 (2018).

[21] K. S. Novoselov, A. K. Geim, S. V. Morozov, D. Jiang, Y. Zhang, S. V. Dubonos, I. V. Grigorieva, and A. A. Firsov, Science 306, 666 (2004).

[22] L. A. Falkovsky and A. A. Varlamov, Eur. Phys. J. B 56, 281 (2007).

[23] L. A. Falkovsky and S. S. Pershoguba, Phys. Rev. B 76, 153410 (2007).

[24] A. H. Castro Neto, F. Guinea, N. M. R. Peres, K. S. Novoselov, and A. K. Geim, Rev. Mod. Phys. 81, 109 (2009).

[25] I. V. Iorsh, I. S. Mukhin, I. V. Shadrivov, P. A. Belov, and Y. S. Kivshar, Phys. Rev. B 87, 075416 (2013).

[26] M. A. Othman, C. Guclu, and F. Capolino, Opt. Express 21, 7614 (2013).

[27] J. S. Gomez-Diaz, M. Tymchenko, and A. Alu, Phys. Rev. Lett. **114**, 233901 (2015).

[28] J. Brouillet, G. T. Papadakis, and H. A. Atwater, Opt. Express **27**, 30225 (2019).

[29] C. H. Lui, K. F. Mak, J. Shan, and T. F. Heinz, Phys. Rev. Lett. **105**, 127404 (2010).

[30] A. Block, M. Liebel, R. Yu, R. Spector, Y. Sivan, F. J. García de Abajo, and N. F. van Hulst, Sci. Adv. **5**, eaav8965 (2019).

[31] J. C. Johannsen, S. Ulstrup, F. Cilento, A. Crepaldi, M. Zacchigna, C. Cacho, I. C. E. Turcu, E. Springate, F. Fromm, C. Raidel, T. Seyller, F. Parmigiani, M. Grioni, and P. Hofmann, Phys. Rev. Lett. **111**, 027403 (2013).

[32] I. Gierz, J. C. Petersen, M. Mitrano, C. Cacho, I. C. E. Turcu, E. Springate, A. Stöhr, A. Köhler, U. Starke, and A. Cavalleri, Nat. Mater. **12**, 1119 (2013).

[33] B. A. Ruzicka, S. Wang, L. K. Werake, B. Weintrub, K. P. Loh, and H. Zhao, Phys. Rev. B **82**, 195414 (2010).

[34] R. Yu, A. Manjavacas, and F. J. García de Abajo, Nat. Commun. **8**, 2 (2017).

[35] D. K. Efetov, R.-J. Shiue, Y. Gao, B. Skinner, E. D. Walsh, H. Choi, J. Zheng, C. Tan, G. Grosso, C. Peng *et al.*, Nat. Nanotechnol. **13**, 797 (2018).

[36] R. Yu, Q. Guo, F. Xia, and F. J. García de Abajo, Phys. Rev. Lett. **121**, 057404 (2018).

[37] N. Kinsey, C. DeVault, J. Kim, M. Ferrera, V. Shalaev, and A. Boltasseva, Optica **2**, 616 (2015).

[38] M. F. Becker, A. B. Buckman, R. M. Walser, T. Lépine, P. Georges, and A. Brun, Appl. Phys. Lett. **65**, 1507 (1994).

[39] M. Z. Alam, I. De Leon, and R. W. Boyd, Science **352**, 795 (2016).

[40] E. J. C. Dias, R. Yu, and F. J. García de Abajo, Light Sci. Appl. **9**, 87 (2020).

[41] K. J. Tielrooij, S. A. J. J. C. W. Song, and, A. Centeno, A. Pesquera, A. Z. Elorza, M. Bonn, L. S. Levitov, and F. H. L. Koppens, Nat. Phys. **9**, 248 (2013).

[42] See Supplemental Material at http://link.aps.org/supplemental/10.1103/PhysRevLett.125.037403 details of the graphene surface conductivity, the reflection coefficients of metamaterials, the thermal dynamics in metamaterials, as well as additional simulations, which includes Refs. [43–49].

[43] F. J. García de Abajo, ACS Photonics **1**, 135 (2014).

[44] V. P. Gusynin, S. G. Sharapov, and J. P. Carbotte, New J. Phys. **11**, 095013 (2009).

[45] T. Sohier, M. Calandra, C.-H. Park, N. Bonini, N. Marzari, and F. Mauri, Phys. Rev. B **90**, 125414 (2014).

[46] P. Yeh, *Optical Waves in Layered Media* (Wiley Online Library, New York, 1988).

[47] C. B. McKitterick, D. E. Prober, and M. J. Rooks, Phys. Rev. B **93**, 075410 (2016).

[48] Q. Guo, R. Yu, C. Li, S. Yuan, B. Deng, F. J. García de Abajo, and F. Xia, Nat. Mater. **17**, 986 (2018).

[49] T. Y. Kim, C.-H. Park, and N. Marzari, Nano Lett. **16**, 2439 (2016).

[50] S. Yuan, R. Yu, C. Ma, B. Deng, Q. Guo, X. Chen, C. Li, C. Chen, K. Watanabe, T. Taniguchi *et al.*, ACS Photonics **7**, 1206 (2020).

[51] W. Lukosz and R. Kunz, J. Opt. Soc. Am. **67**, 1607 (1977).

[52] L. Novotny and B. Hecht, *Principles of Nano-Optics* (Cambridge University Press, New York, 2006).

[53] F. J. García de Abajo, Rev. Mod. Phys. **82**, 209 (2010).

[54] B. Barwick, D. J. Flannigan, and A. H. Zewail, Nature (London) **462**, 902 (2009).

[55] A. Feist, K. E. Echternkamp, J. Schauss, S. V. Yalunin, S. Schäfer, and C. Ropers, Nature (London) **521**, 200 (2015).

[56] L. Piazza, T. T. A. Lummen, E. Quiñonez, Y. Murooka, B. Reed, B. Barwick, and F. Carbone, Nat. Commun. **6**, 6407 (2015).

[57] G. M. Vanacore, I. Madan, G. Berruto, K. Wang, E. Pomarico, R. J. Lamb, D. McGrouther, I. Kaminer, B. Barwick, F. J. García de Abajo *et al.*, Nat. Commun. **9**, 2694 (2018).

[58] R. Dahan, S. Nehemia, M. Shentcis, O. Reinhardt, Y. Adiv, K. Wang, O. Beer, Y. Kurman, X. Shi, M. H. Lynch *et al.*, arXiv:1909.00757.

[59] F. J. García de Abajo and M. Kociak, Phys. Rev. Lett. **100**, 106804 (2008).

[60] P. A. Belov and M. G. Silveirinha, Phys. Rev. E **73**, 056607 (2006).

[61] P. A. Belov, C. R. Simovski, and P. Ikonen, Phys. Rev. B **71**, 193105 (2005).

[62] A. Salandrino and N. Engheta, Phys. Rev. B **74**, 075103 (2006).

[63] K.-i. Maki and C. Otani, Opt. Express **16**, 10158 (2008).

[64] T. Cao, G. Zheng, S. Wang, and C. Wei, Opt. Express **23**, 18029 (2015).

[65] P. M. Johnson, A. F. Koenderink, and W. L. Vos, Phys. Rev. B **66**, 081102(R) (2002).

[66] C.-Y. Jin, R. Johne, M. Y. Swinkels, T. B. Hoang, L. Midolo, P. J. Van Veldhoven, and A. Fiore, Nat. Nanotechnol. **9**, 886 (2014).

[67] G. Ctistis, E. Yuce, A. Hartsuiker, J. Claudon, M. Bazin, J.-M. Gérard, and W. L. Vos, Appl. Phys. Lett. **98**, 161114 (2011).